

# Estimation of aboveground biomass and carbon in palustrine wetland using bands and multispectral indices derived from optical satellite imageries PlanetScope and Sentinel-2A

Tássia Fraga Belloli<sup>1</sup>,<sup>a,\*</sup> Laurindo Antonio Guasselli<sup>1</sup>,<sup>a</sup>  
Tatiana Mora Kuplich<sup>1</sup>,<sup>a,b</sup> Luis Fernando Chimelo Ruiz<sup>1</sup>,<sup>c</sup>  
Diniz Carvalho de Arruda,<sup>a</sup> Cecilia Balsamo Etchelar<sup>1</sup>,<sup>a</sup> and  
João Delapasse Simioni<sup>a</sup>

<sup>a</sup>Federal University of Rio Grande do Sul, State Center for Research in Remote Sensing and Meteorology, Porto Alegre, Brazil

<sup>b</sup>National Institute for Space Research, Southern Regional Centre, Santa Maria, Brazil

<sup>c</sup>Nucleus for Research and Development of Innovative Technologies, Santos Lab, Rio de Janeiro, Brazil

**Abstract.** Facing the climate change and anthropogenic activities that have been discharging a large proportion of carbon dioxide (CO<sub>2</sub>) into the atmosphere, wetlands stand out as an important sink for CO<sub>2</sub> that is fixed in plant biomass and peatlands. Therefore, quantifying and monitoring wetland biomass is of great importance to preserve carbon stocks. This study aims to explore the potential of multispectral bands and vegetation indices (VIs) derived from PlanetScope and Sentinel-2A sensors to estimate of aboveground biomass (AGB) and organic carbon in AGB (Corg) in the emergent vegetation of a palustrine wetland. We use correlation analysis and linear regression models to examine the relationships between spectral and biophysical variables and verify the best predictor spectral variables for AGB and Corg. *Scirpus giganteus* vegetation was sampled in the Banhado Grande wetland, in southern Brazil. The VIs were best correlated and preferred as predictor variables. The most accurate model used data from the PlanetScope sensor and VI of photochemical reflectance. Both sensors showed potential for pixel-based estimates of AGB and Corg due to their low RMSE values and their contribution as predictors of biophysical variables, which can contribute to opening new avenues in scientific research focusing on the management, monitoring, and conservation of marshes and your ecosystem service of carbon sink. © 2022 Society of Photo-Optical Instrumentation Engineers (SPIE) [DOI: [10.1117/1.JRS.16.034516](https://doi.org/10.1117/1.JRS.16.034516)]

**Keywords:** aboveground biomass; blue carbon; remote sensing; marsh; predictive models.

Paper 220220G received Apr. 12, 2022; accepted for publication Jul. 15, 2022; published online Aug. 4, 2022.

## 1 Introduction

Coastal wetland ecosystems, such as mangroves, marshes, and saltmarshes, provide a variety of ecosystem services. Among these, we highlight the capture of atmospheric carbon dioxide (CO<sub>2</sub>) by plant biomass, and its storage as organic matter in substrates and soils.<sup>1-3</sup> As a natural carbon sink, this function makes them critical for the mitigation of natural and anthropogenic climate change in front of exponential increases in atmospheric CO<sub>2</sub> in recent decades.<sup>4,5</sup> This ecosystem service of coastal wetlands has been referred to in the literature as blue carbon.<sup>6-9</sup> These studies contribute to the management of wetlands and conservation of their biogeochemical processes.<sup>4,10</sup>

Assessing carbon storage in the biomass of vegetated ecosystems is critical for carbon offset initiatives, such as reducing emissions from deforestation and degradation (REDD+) and for

---

\*Address all correspondence to Tássia Fraga Belloli, [tassiabelloli@gmail.com](mailto:tassiabelloli@gmail.com)

facilitating a low-carbon economy.<sup>11,12</sup> This assessment is also important for blue carbon research and for the conservation of coastal wetlands and their ecosystem services.<sup>13</sup> Furthermore, these biophysical variables are primary indicators of wetlands physiological status and your monitoring should be performed regularly to assess the health of the wetland ecosystem.<sup>14</sup>

These measurements are usually obtained on site, by sampling a small area, based on replicated squares, to estimate aboveground biomass (AGB). Dry biomass values are converted into organic carbon (Corg) storage using a generalized conversion factor and multiplied by the vegetation extent to calculate total aboveground carbon storage.<sup>15–17</sup> This is a suitable approach in situations where the structural form of the vegetation is more homogeneous, such as extensive monospecific stands,<sup>18</sup> but it is less precise when there is high species diversity with variable distribution.<sup>19</sup>

Due to difficulties in accessing wetlands, many studies seek to develop innovative and effective methodologies, based on integration of geographical information system and remote sensing (RS) techniques to map, classify, monitor,<sup>20</sup> and analyzing substantial biophysical parameters in the context of regional and global scales.<sup>21,22</sup>

Compared with traditional methods, RS technology allows for a quick, accurate, and less destructive estimation of the vegetation biomass and carbon of wetlands, as *in situ* data are still needed to calibrate models. Wetland biomass studies have mainly focused on AGB and carbon sinks, using optical remote sensing, synthetic aperture radar (SAR) or a combination thereof, and light detection and ranging (LiDAR). These are the three main methods for such efforts.<sup>17,23</sup>

Other sensors, from either airborne platforms or an unmanned aerial vehicle (UAV) or a high spatial resolution, have been used to map and estimate AGB,<sup>24,25</sup> have an imaging system that can potentially replace traditional aerial surveys, and offer better techniques for monitoring blue carbon habitats. Datasets produced by RS-based UAV with high spatial resolution of 2 to 5 cm can detect changes in blue carbon species compositions and can be mapped in detailed 2D and 3D.<sup>26</sup> High spatial resolution RS images and LiDAR data are often restricted by their limited spatial and temporal coverage and, because of this, are most commonly used for studies in small-scale wetlands.<sup>27</sup>

Among the available sensor systems, the optical systems are the most used so far to model AGB and Corg in wetlands, especially those of medium spatial resolution (range of 4 to 30 m).<sup>17,28</sup> Optical RS method uses the spectral characteristics of plants that are mostly related to electromagnetic radiation (ER) absorption by plant pigments in the visible region of the spectrum (0.4 to 0.72 nm), ER reflectance in the near infrared (NIR) region (0.72 to 1.1 nm) as a function of cell structure, and absorption by water in the mid infrared region (1.1 to 3.2 nm).<sup>29</sup>

Applying RS techniques in wetland is more complex than in terrestrial vegetation. Furthermore, the occurrence of flood pulses introduces greater variability in reflectance values due to the mixing of plant and water signals. This mixing usually results in a decrease in total reflected radiation, especially in the near to mid infrared regions, where water absorption is stronger.<sup>30</sup> Red-edge locations transfers may also occur and eventually reduce the effects of red-edge type vegetation indices (VIs) to detect growing vegetation.<sup>31</sup> The degree of soil moisture in wetlands also decreases the intensity of the spectral response and the values of VIs, such as normalized difference vegetation index (NDVI).<sup>32</sup>

Indices particularly based on the red and NIR bands are sensitive to the condition of green leaf vegetation (amount of chlorophyll), the structure of the vegetation and photosynthetically active radiation. Due to these characteristics, they are often used in wetlands, in studies related to photosynthesis and related to field data of biophysical variables, such as AGB and Corg,<sup>33–35</sup> water balance, and other related processes.<sup>36</sup> However, these VIs were established mainly for terrestrial vegetation.

Among the VIs developed for wetland vegetation, the NDVI adaptations that replace the red spectral band by the blue spectral band, such as the indices proposed in Ref. 37 stand out. The authors applied normalized difference aquatic vegetation index (NDAVI) and water adjusted vegetation index (WAVI) VIs in a large set of hyperspectral and multispectral sensor images, with spatial resolutions from 2 to 90 m. They concluded that these VIs provided better separability characteristics compared to those obtained by ground-based VIs over varied vegetation types and conditions, and that NDAVI and WAVI values were superior to NDVI and soil modified vegetation index (SAVI). They also ensure that the integration of these indices and *in situ*

data (nutrients, pigments, and biomass) can contribute to a better understanding of vegetation dynamics in aquatic ecosystems and to management and conservation programs.

RS methods for modeling AGB and Corg make use of in situ data (biomass) to “train” the algorithm and develop a set of rules or models from the satellite images.<sup>38</sup> These models can be divided into two types, machine learning (ML)-based models and spectral variables (SV)-based linear regression models. ML-based models often perform better when predicting the AGB of coastal wetlands compared to linear regression models,<sup>23,39</sup> but need a larger number of field samples to train and validate the models and are more complex to apply. Thus, the difficulty of acquiring sufficient AGB samples from coastal wetlands is a limiting factor for application of these models.

However, the linear regression models, with a few field samples and several RS spectral data, achieve good results and are widely used to estimate AGB and Corg of coastal wetlands. As checked in Ref. 34 in predicting AGB for the Bohami Rim coastal wetland, China, using a linear regression model based on multiple data sets (seven independent variables from 23 metrics derived from Sentinel-1 SAR data and Sentinel-2 images, topography, and climate data), which obtained a root mean square error (RMSE) and  $r$  value of 188.32 g/m<sup>2</sup> and 0.74, respectively. From the AGB map generated with the model, the authors generated an AGB carbon stock map.

Among the main sensors used in studies of wetland vegetation and estimation of AGB in blue carbon ecosystems, highlight the Landsat thematic mapper (TM), enhanced thematic mapper (ETM), and operational land imager (OLI) sensors<sup>17,28</sup> as the best option for large scale AGB and Corg sinks modeling.<sup>7,22</sup> Many researchers still prefer medium-resolution satellite images for measuring AGB over long periods and at large areas.<sup>27</sup> Thus, high resolution satellite data is still under-utilized. More studies are still using high-resolution satellite sensors in mapping and estimation of blue carbon multi-species.<sup>17</sup>

The availability of Earth observation satellites such as the European Space Agency (ESA) Sentinel series Sentinel-1 (radar) and Sentinel-2 (optic), open access, and operational since 2015 provides opportunities to assess AGB modeling capabilities and carbon stock of palustrine wetlands, achieving good results, with  $R^2 = 0.63$  and an RMSE of 169.68 g/m<sup>2</sup><sup>40</sup> and in herbaceous wetlands with an accuracy of 75.4%.<sup>41</sup>

Sentinel-2 is a terrestrial monitoring constellation of two identical satellites (2A and 2B) with new spectral capabilities and a five day revisit time. It carries optical sensors in the visible and infrared ranges, for a total of 13 spectral bands with 10-, 20-, and 60-m spatial resolution.<sup>42</sup> It is known as the first commercial satellite with a red edge band in addition to the visible and infrared bands. Around the same time, images from the PlanetScope sensor, launched in 2014, begin to be explored in wetlands. The PlanetScope sensor, a CubeSat developed by Planet Labs Inc. (San Francisco, California), has fewer bands than the Sentinel sensor (blue, green, red, and infrared) but has 3-m spatial resolution and daily revisits.<sup>43</sup>

With this new moderate-resolution satellite systems, the estimation of biophysical data can be obtained by improved sensors, with shorter revisiting time. The efficiency of multispectral bands and VIs derived from PlanetScope and Sentinel-2 sensors was separately evaluated in Ref. 44 to predicting mangrove biomass and generated prediction models through conventional linear regression and multivariate regression. Higher coefficient of determination ( $R^2$ ) values were obtained using multispectral band predictors for Sentinel-2 ( $R^2 = 0.89$ ) and Planetscope ( $R^2 = 0.80$ ).

NDVI images derived from PlanetScope were tested in Ref. 35 to be reliable proxies for temporal variations of AGB and carbon content in a saltmarsh ecosystem in Jervis Bay National Park. The authors found a strong correlation ( $r = 0.78$ ;  $p < 0.001$ ) between the aboveground carbon content extracted from a map created using the ArborCam image and the NDVI extracted from PlanetScope image.

To date, the number of studies that have explored the relationship and prediction of AGB and Corg in wetlands using the PlanetScope sensor is much lower than those using the Sentinel-2 sensor. For ecosystems with predominantly emergent vegetation such as marsh, saltmarsh, or palustrine wetlands, this number is even smaller. This demonstrates the need and gaps that still exist to explore the spectral properties of both sensors and their relationship with this biophysical variables explicit in these ecosystems.

Moreover, so far, no previous studies have compared the performance of these satellite data for emerging wetland vegetation, using prediction models developed from the same on-site

collected data, with emphasis on the common bands and VIs that can be derived from these systems. Thus, the aim of this study is to explore the potential of multispectral bands and VIs derived from PlanetScope and Sentinel-2A sensors as predictors of AGB and Corg in the emergent vegetation of a palustrine wetland.

The relations between AGB and Corg and the SV of the sensors are addressed as from correlation analysis. Predictive models were performed from the SV best correlated with the biophysical parameters using simple and multivariate linear regression algorithms. The accuracy of the best models was validated with sample data obtained in the experimental units. Moreover, this study contributes with the provision of the most relevant bands and VIs of the Sentinel-2 and PlanetScope satellite images to obtain optimal accuracy in the estimation of AGB and carbon sinks in a palustrine wetland in southern Brazil.

## 2 Materials and Methods

### 2.1 Study Area

The study area is located in the Banhado Grande (BG) wetland, between the municipalities of Glorinha, Santo Antônio da Patrulha and Viamão (29°57'S; 50°41'W), east of the state of Rio Grande do Sul (Fig. 1). BG is a palustrine environment integrated with the Banhado Grande Environmental Protection Area (EPABG) for sustainable use, comprising marsh areas, flood plains, and rice fields that become connected in periods of large flooding pulses.<sup>45</sup>

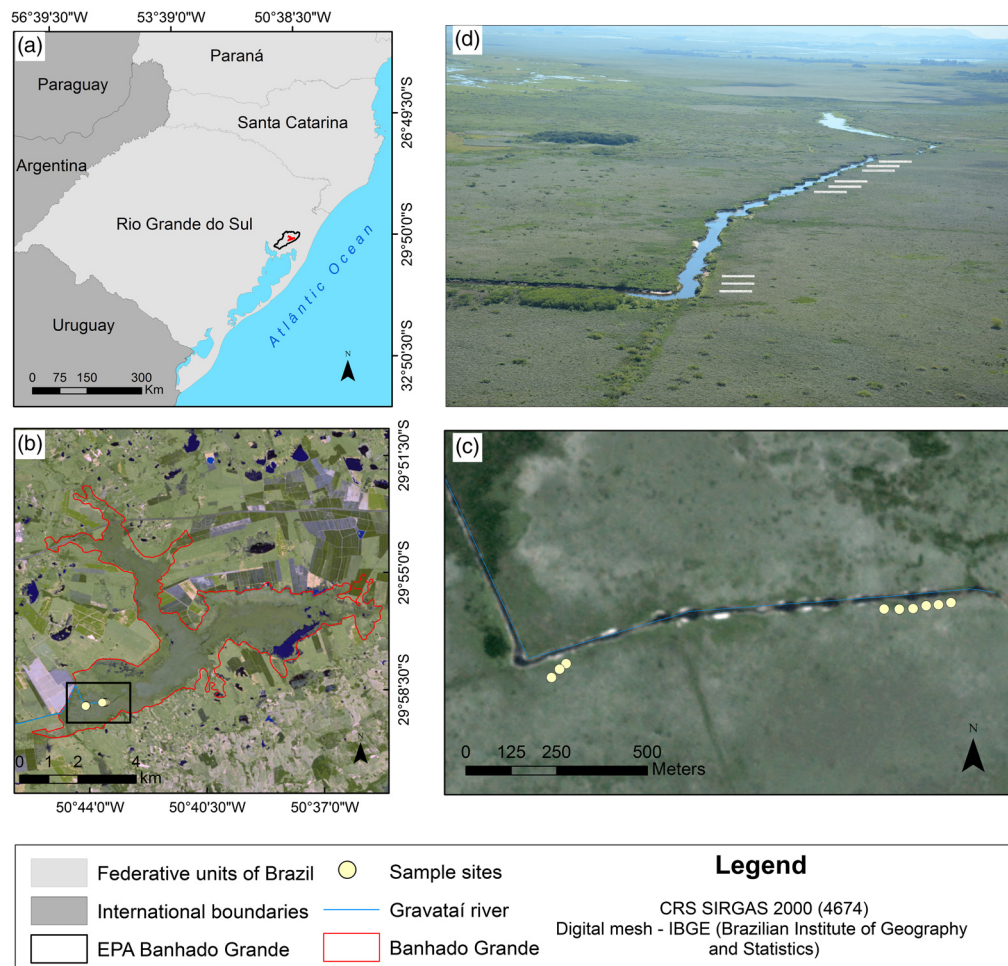


**Fig. 1** Study area and sample sites: (a) location of BG and EPABG in Rio Grande do Sul; (b) white dots indicating sample sites in BG; and (c) simplified projection image of sample sites.

In the vegetation cover of the experimental area, aquatic macrophytes predominate, comprising the emerging species *Scirpus giganteus*, with the most representative area and coverage in monodominance in the wetland.<sup>46,47</sup> It occurs in areas with a presence of active peat bogs,<sup>48,49</sup> extending for ~1507 ha.<sup>47</sup>

The study area is located in the geomorphological region of the Inner Coastal Plain, in a flat area with altimetry of up to 20 m. The lithology is predominantly sedimentary environments with heterogeneous peat, interconnected by floodplain deposits composed of silt-clay sand.<sup>50</sup> The location is characterized by a humid subtropical climate, with no defined dry and rainy season. Rainfall ranges from 1700 to 1800 mm per year, distributed across 100 to 120 days of rain. The mean annual temperature varies between 17°C and 20°C.<sup>45,51</sup>

## 2.2 Field Data Collection

Biomass samples were collected at nine sites throughout one annual cycle in 2018, at the end of the summer (March 14), winter (August 17), and spring (November 22) seasons. At each site, three sample locations were randomly selected; in total, 27 biomass samples were collected. These sites were selected because they are accessible, in addition to contemplating an extensive area with monodominance of *Scirpus giganteus*.

The sampling scheme was designed so that each sample sites corresponds to a transect similar to a 20 m by 20 m Sentinel pixel. The sample sites were fixed with stakes, spaced at least 40 m apart, aligned in the north-south direction, positioned with Global Positioning System (GPS) equipment Etrex Legend model, with a margin of error of 3 m. The sample sites were positioned in large areas with monospecific predominance of *Scirpus giganteus* [Fig. 2(a)] so that the collection of reflectance data in the pixels of the images did not occur outside the areas with the desired plants, due to possible errors in GPS positioning and of the sensors.

Collections were carried out according to the guidelines shown in Refs. 16 and 52. Only areas with monodominance of *Scirpus giganteus* were sampled [Fig. 2(b)]. A 50 cm × 50 cm quadrat (0.25 m<sup>2</sup>) was placed over the plants and plant matter was clipped to the soil surface. The plants were bagged and returned to the laboratory where samples were dried in an oven at 60°C for 72 h or until a constant weight was reached to obtain the dry biomass. The material was weighed on a precision scale to obtain the dry weight expressed in grams per m<sup>2</sup>.

Corg concentration was obtained with the Walkley Black wet combustion method.<sup>53</sup> This method shows the organic carbon content (%) in 100 g of dry weight of biomass. The conversion of dry biomass weight (g/m<sup>2</sup>) to Corg stocks (g/m<sup>2</sup>) was done based on direct proportion.<sup>16,54</sup> In the rest of the text, we will express AGB as the amount of dry biomass (g/m<sup>2</sup>) above ground and Corg as the organic carbon content (g/m<sup>2</sup>) present in the AGB.

Descriptive [minimum, maximum, mean, and standard deviation and coefficient of variation (CV%)] and bivariate (Levene) statistics of the samples were calculated using the statistical program SPSS 18.0.<sup>55</sup>



**Fig. 2** Collection of the vegetation *Scirpus giganteus*: (a) image with point of a sample site and (b) image after the vegetation cut, date: March 14, 2018, BG – RS. Source: Author.

**Table 1** Image acquisition and field data collection dates.

Sensor	March/2018	August/2018	November/2018
Sentinel-2A	March 11	August 28	November 16
PlanetScope	March 13	August 17	November 21
Field data collection	March 14	August 17	November 22

### 2.3 Satellite Data and Image Processing

Sentinel-2A and PlanetScope data were obtained as close as possible to the vegetation collection dates (Table 1). The Sentinel-2A image was obtained from the Copernicus website,<sup>56</sup> in the 13 bands of the multispectral instrument (MSI) sensor, with pre-processing level 1C. Of these, the visible (blue, green, and red) and NIR bands have a spatial resolution of 10 m; the Red Edge (RE5, RE6, RE7, and RE8A) and shortwave infrared (SWIR1 and SWIR2) bands have a spatial resolution of 20 m; and bands 1, 9, and 10 have a spatial resolution of 60 m<sup>42</sup> but were not used since those sensors are designed to detect coastal aerosols, water vapor, and cirrus cloud radiation, respectively.

The images are orthorectified, georeferenced, and radiometrically calibrated, with an atmospheric correction applied to top-of-atmosphere. The images were pre-processed to level 2A to remove atmospheric effects and convert pixel values to surface reflectance. Pre-processing was performed using the Sen2Cor tool from ESA,<sup>57</sup> on the Sentinel Application Platform (SNAP). The 2A level bands were stacked and resampled to 10-m spatial resolution using the nearest method, in the SNAP geometric operation tool.

PlanetScope images were obtained from the Planet Platform,<sup>58</sup> Ortho Scene product with four spectral bands, 3B pre-processing level and 3-m spatial resolution. The Ortho Scene product is distributed in images with radiance values (Planet Analytic product) and reflectance values (Planet Surface Reflectance–SR). The SR product is derived from the Planet Analytic product, the bands are co-acquired, orthorectified, and georeferenced, with radiometric calibration in surface reflectance using the 6S algorithm, V2.1. The SR product ensures consistency in all weather conditions, minimizing the uncertainty of the spectral response in time and location.<sup>43</sup>

### 2.4 Vegetation Indices

About 10 VIs (Table 2) were analyzed as predictor variables for AGB and Corg. Among the VIs, NDVI is often used to estimate vegetation biomass in wetlands<sup>33,67</sup> and in studies related to photosynthesis, carbon stocks, water balance, and other plant-related processes. This VI is sensitive to green leaf vegetation and photosynthetically active radiation.<sup>68</sup>

We use specific VIs for wetland vegetation, such as the NDAVI and the WAVI, which are versions of the NDVI and EVI adapted for wetlands by replacing the red spectral band by the blue spectral band.

To estimate Corg, the indices of photochemical reflectance (sPRI) and integrated index (CO<sup>2</sup>flux) are sensitive to changes in carotenoid pigments in leaves, indicative of the efficiency of the use of photosynthetic light or the level of carbon dioxide stored by vegetation. CO<sup>2</sup>flux is an integrated index, formed by the PRI and NDVI VIs, which represent the light use efficiency in photosynthesis and the vigor of photosynthetically active vegetation, respectively.

The use of indexes formulated with red edge bands has been growing since the Sentinel-2 and RapidEye satellites missions. Studies have addressed the important relationship between reflectance and chlorophyll and other nutrients present in the plant cell structure<sup>69,70</sup> with the foliar area index<sup>71</sup> and plant biomass.<sup>44,72</sup> Variations of the NDVI index were tested with combinations of bands in the visible, red edge, and NIR spectral ranges of Sentinel-2 (VIs Normalized Difference Red Edge – NDRE1 to NDRE3). Because CO<sub>2</sub>Flux is an integrated index, a formulation was also tested by replacing NDVI by NDAVI, if NDAVI had higher reflectance values than NDVI. The VIs are based on the band mathematics of the sensors' reflectance images and were calculated in Qgis v 12.3 software.

**Table 2** Vegetation indices used in the study.

VIs	Equation	References
NDVI—normalized difference	$NDVI = \frac{(\rho_{NIR} - \rho_{Red})}{(\rho_{NIR} + \rho_{Red})}$	Rouse et al. <sup>59</sup> and Tucker <sup>60</sup>
NDAVI—aquatic by normalized difference	$NDAVI = \frac{(\rho_{NIR} - \rho_{Blue})}{(\rho_{NIR} + \rho_{Blue})}$	Villa et al. <sup>61</sup>
WAVI—adjusted to water	$WAVI = (1 + L) \frac{(\rho_{NIR} - \rho_{Blue})}{(\rho_{NIR} + \rho_{Blue} + L)}$	Villa et al. <sup>37</sup>
NDRE1—normalized difference red edge 1	$NDRE1 = \frac{(\rho_{RE6} - \rho_{RE5})}{(\rho_{RE6} + \rho_{RE5})}$	Gitelson and Merzlyak <sup>62</sup>
NDRE2—normalized difference red edge 2	$NDRE2 = \frac{(\rho_{RE7} - \rho_{RE5})}{(\rho_{RE7} + \rho_{RE5})}$	Barnes et al. <sup>63</sup>
NDRE3—normalized difference red edge 3	$NDRE3 = \frac{(\rho_{RE5} - \rho_{RE4})}{(\rho_{RE5} + \rho_{RE4})}$	Gitelson and Merzlyak <sup>62</sup>
sPRI—photochemical reflectance	$PRI = \frac{(\rho_{Blue} - \rho_{Green})}{(\rho_{Blue} + \rho_{Green})}$ $sPRI = \frac{(PRI + 1)}{2}$	Gamon et al. <sup>64</sup> and Rahman et al. <sup>65</sup>
CO <sub>2</sub> Flux—integrated	CO <sub>2</sub> Flux = (NDVI X sPRI)	Rahman et al. <sup>65</sup> and Baptista <sup>66</sup>
CO <sub>2</sub> Flux—integrated NDAVI	CO <sub>2</sub> FluxNDAVI = (NDAVI X sPRI)	Author

Note:  $\rho_{NIR}$  = near infrared reflectance;  $\rho_{RE}$  = red edge reflectance;  $\rho_{Blue}$  = blue reflectance;  $\rho_{Green}$  = green reflectance;  $\rho_{Red}$  = red reflectance. Value assumed by the algorithm: WAVI:  $L = 0.5$ .

### 2.5 Statistical Analysis

The spectral values of the bands and VIs were obtained from the pixels corresponding to the points of each sample site on BG. For the automatic extraction of the values, the point sampling tool, available in the QGIS software, was used. Descriptive (minimum, maximum, mean, error, and standard deviation) and multivariate (Pearson, simple and multiple linear regression, one-way ANOVA and Tukey test) statistics were generated. Due to the characteristics of the database and to strengthen the relationship between data, the AGB and Corg variables were transformed to a natural logarithm scale for the correlation and regression application.

To identify the bands and VIs with the most significant correlation and contribution as predictor variables, a correlation matrix of the biophysical data and the values corresponding to the bands and VIs in each sensor was generated, using Pearson’s correlation coefficient ( $r$ ), considering significant  $p < 0.05$  (95% CI). The data were analyzed using the SPSS 22.0 and RStudio 1.4.1106 programs.

The method used to select the variables for the regression models was the Hierarchical with block entry, in which predictors are selected by the researcher based on their order of importance to predict the output variable.<sup>73</sup> The hierarchical criterion used was to first insert the variables with the highest and significant correlation with the output variables (AGB and Corg). After entering these predictors, predictors with lower correlation are added, following the hierarchical order.

The models used to estimate AGB and Corg were obtained after a multiple first-order linear regression, according to the (generic) equation below, Eq. (1)

$$y = (\beta_0 + \beta_1.x_1 + \beta_2.x_2 + \beta_n.x_n.) + \epsilon, \tag{1}$$

where  $y$  are the biophysical variables to be estimated,  $x$  are the independent variables (spectral bands and VIs),  $\beta_0, \beta_1, \beta_2,$  and  $\beta_n$  are unknown coefficients and  $\epsilon$  is the model’s random error or residual.

If the multiple regression did not meet the assumptions for a satisfactory regression, a simple linear regression, Eq. (2), was used

$$y = (\beta_0 + \beta_1.x_1) + \epsilon.e. \tag{2}$$

For all equations, the necessary assumptions for a satisfactory regression were observed:  $p$ -value, multicollinearity, homogeneity, independence of errors, and normality of residuals.

The performance of the models was evaluated by the Student's *t*-test and ANOVA with a significance level of  $p < 0.005$ , for the best value of the coefficient of determination ( $R^2$ ) and adjusted coefficient of determination ( $R^2_{adj}$ ). To assess the accuracy of the models, the parameters  $R^2_{adj}$  and RMSE were used. SPSS determines the value of  $R^2_{adj}$  using the Wherry equation.<sup>73</sup> In a final step, the highest performing model were applied to the entire study area to generate AGB and Corg maps in the area covered by *Scirpus giganteus* in the BG marsh, using the Rasterio Python library in Python 3.

### 3 Results and Discussion

#### 3.1 Analysis of the Correlation between the Biophysical Data and Spectral Data

The field-measured data and its statistics are shown in Table 3. The mean AGB of the field-measured ranged between  $598.76 \text{ g/m}^2 \pm 70.89$  ( $\pm$  standard error) and  $862.98 \text{ g/m}^2 \pm 87.83$ . The minimum and maximum values were 340.24 and 1289.28  $\text{g/m}^2$ , respectively. During the three campaign of field collections, no preferential periods of senescence or change in plant growth (height) were observed. However, new leaves were observed in larger quantities in the last field collection. Flowering development was not observed either. Based on the homogeneity of variances test (Levene's test), no significant differences were observed in the variance of the AGB and Corg values between the collection dates (df 2, F 3.28,  $p < 0.005$ ).

The dynamics of *Scirpus giganteus* biomass was analyzed in Refs. 74 and 75 on an island in the lower delta of the Paraná River, Argentina. The authors observed high leaf turnover in the

**Table 3** Field-measured data and its descriptive statistics.

Sample sites\Date	AGB ( $\text{g/m}^2$ )			Corg ( $\text{g/m}^2$ and %)		
	March 14	August 17	November 22	March 14	August 17	Nov 22
1	686.28	587.08	1076.28	281.37 and 41%	234.832 and 40%	441.27 and 41%
2	556.44	340.24	855.28	233.7 and 42%	142.90 and 42%	350.66 and 41%
3	671.16	433.08	719.2	288.6 and 43%	173.23 and 40%	280.49 and 39%
4	651.04	477.88	1289.28	273.44 and 42%	200.71 and 42%	502.82 and 39%
5	611.68	503.68	649.88	256.90 and 42%	206.51 and 41%	259.95 and 40%
6	443.96	675.08	1105.08	190.9 and 43%	276.78 and 41%	442.03 and 40%
7	636.08	683.28	765.84	267.15 and 42%	293.81 and 43%	336.97 and 44%
8	618.88	1079.08	422.92	266.12 and 43%	442.42 and 41%	173.40 and 41%
9	610.96	609.48	883.08	256.6 and 42%	249.89 and 41%	406.22 and 46%
Min	443.96	340.24	422.92	190.9 and 41%	142.9/ 40%	173.4/ 39%
Max	686.28	1079.08	1289.28	288.6/ 43%	442.42/ 43%	502.82/ 46%
Mean	609.61	598.76	862.98	257.2/ 42%	246.79/ 41%	354.87/ 41%
SE	24.28	70.89	87.83	9.83/ 0.22	29.22/ 0.32	34.84/ 0.77
Std	72.84	212.68	263.5	29.5/ 0.66	87.67/ 0.97	104.52/ 2.33
Reference values	377 a 500 $\text{g/m}^2$ <sup>74,75</sup>			370 a 702 $\text{g/m}^2$ e 40% <sup>76,77</sup>		

Note: SE: standard error, Std: standard deviation.

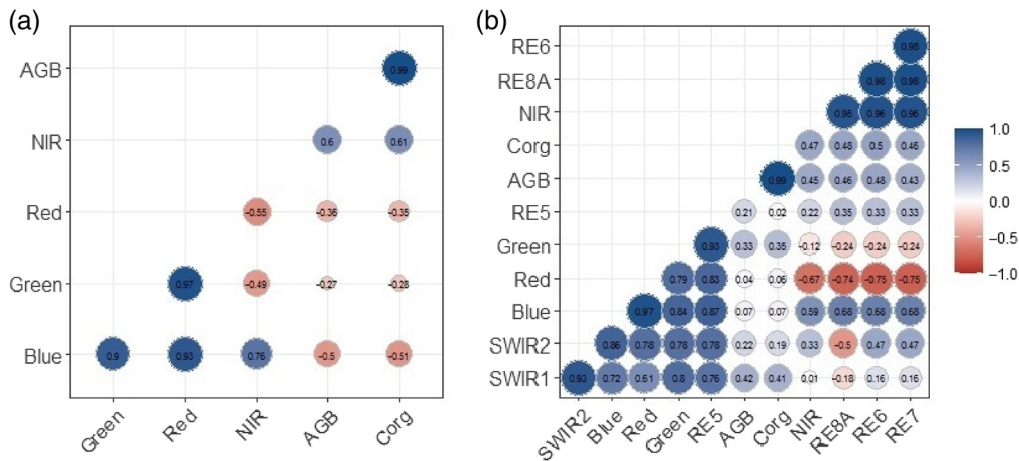


**Fig. 3** Pearson correlation coefficient matrix between spectral bands and biophysical variables in each sensor. (a) PlanetScope sensor and (b) Sentinel-2A sensor. AGB: aboveground biomass; Corg: organic carbon; red: band corresponding to red in the visible spectrum; NIR: band corresponding to near infrared; RE: bands corresponding to the red edge band; and SWIR: band corresponding to shortwave infrared.

*Scirpus giganteus* area, with new green leaves even during the winter months. They also did not identify a seasonal trend of senescence or increase in biomass, but they did verify leaf growth throughout the annual cycle. Mean biomass values ranged between 377 and 500 g/m<sup>2</sup> and were lower than the mean values found in our study.

As for the Corg content in the biomass, values around 40% were found, with a minimum of 39% and a maximum of 46%. Mean Corg ranged between 246.79 ± 29.22 and 354.87 g/m<sup>2</sup> ± 34.84. In research studies on blue carbon, the most prevalent method for estimating organic carbon is burning the dry biomass samples. Among the factors for conversion of biomass into blue carbon used in geospatial-based studies, 50% is the factor frequently adopted for mangrove habitats<sup>17</sup> and for marshes values between 34%<sup>76</sup> and 48%.<sup>77</sup> In general, they are balanced at 40% of the dry biomass weight for emerging vegetation,<sup>54,78,79</sup> similar to the values verified for *Scirpus giganteus* in our study.

The relations between AGB and Corg and the SV of the sensors are shown in Fig. 3 and Table 4, as from correlations analysis. Note that the variables AGB and Corg were strongly correlated ( $r = 0.99$ ) since the Corg amount derives from a value that is proportional to the AGB weight. This reflected a similar correlation for both variables in relation to the image bands and VIs evaluated.

When comparing the visible and NIR spectral bands, it was verified that the bands that showed the best and more significant correlation between the biophysical and spectral variations in one sensor were not the same bands observed in the other, but in both the NIR band obtained significant correlation ( $p < 0.05$ ). PlanetScope’s NIR and Blue bands showed significant and the highest correlations (NIR = 0.60; 0.61 and blue = -0.50; -0.51;  $p < 0.05$ ) while the lowest correlation occurred with the green band. The same results were reported in Ref. 44 who showed that the NIR band was the most effective, for both Planetscope ( $r = 0.44$ ) and RapidEye ( $r = 0.25$ ), in predicting mangrove biomass while the green band had the lowest correlation.

For the Sentinel-2A data, the red edge bands (RE6 and RE8) stood out with best and significant  $r$  values for AGB and Corg, respectively (RE6 = 0.48; 0.50 and RE8 = 0.46; 0.48;  $p < 0.05$ ). The blue and red bands resulted in the lowest  $r$  values ( $r = 0.07$  and 0.04).

The inverse correlation with the blue band of the PlanetScope sensor and the no significant correlations in the blue and red bands of the Sentinel-2A sensor are due to the higher absorption of radiation by vegetation pigments (chlorophyll, carotenoids, and xanthophyll) in these regions of the spectrum since absorption increases proportionally with the content of these pigments.<sup>29</sup> They indicate photosynthetic efficiency or the rate of carbon dioxide used and stored by the vegetation.<sup>64,65</sup> Radiation absorption is proportional to the increase in AGB in this region of the spectrum.<sup>80</sup>

**Table 4** Pearson Correlation coefficient and p-values for AGB and Corg with spectral bands.

Bands	PlanetScope sensor				Sentinel-2 sensor			
	AGB		Corg		AGB		Corg	
	<i>r</i>	<i>p</i>	<i>r</i>	<i>p</i>	<i>r</i>	<i>p</i>	<i>r</i>	<i>p</i>
BLUE	-0.50	0.011	-0.51	0.009	0.07	0.737	0.07	0.742
GREEN	-0.27	0.207	-0.28	0.182	0.33	0.105	0.35	0.085
RED	-0.36	0.092	-0.35	0.083	-0.04	0.848	-0.06	0.786
NIR	0.60	0.002	0.61	0.001	0.45	0.022	0.47	0.018
RE 5	—	—	—	—	0.21	0.317	0.24	0.244
RE 6	—	—	—	—	0.48	0.015	0.50	0.011
RE 7	—	—	—	—	0.43	0.033	0.46	0.022
RE 8A	—	—	—	—	0.46	0.021	0.48	0.015
SWIR 11	—	—	—	—	0.42	0.036	0.41	0.044
SWIR 12	—	—	—	—	0.22	0.299	0.19	0.354

Note: *p*-value < 0.05 is significant.

An inverse spectral response occurs in the NIR region, where reflectance increases with increasing AGB. This inversion occurs due to the significant correlation of the NIR bands of the two sensors, followed by the red edge bands. The red edge bands also reflect the chlorophyll content related to the vigor of photosynthetically active vegetation.<sup>70,81,82</sup>

The red edge bands B6, B7, B8, and B8A were strongly correlated with Grassland AGB in the Lake Shengjin wetland, China, being the most important ones for biomass prediction models compared to other Sentinel bands, as shown in Ref. 72 The red edge bands are effective for monitoring vegetation and can both quantify AGB and map plant communities in wetlands.<sup>83</sup>

Consequently, the VIs generated from the bands with more significant correlation also achieved the best correlation coefficient among the VIs. Figure 4 and Table 5 present the correlation between the VIs and biophysical variables. For the PlanetScope sensor, the sPRI VIs showed the best and more significant correlation for AGB and Corg, *r* = 0.66 and 0.68; *p* < 0.05, followed by CO<sub>2</sub>FluxNDAVI, *r* = 0.61; 0.62; *p* < 0.05.

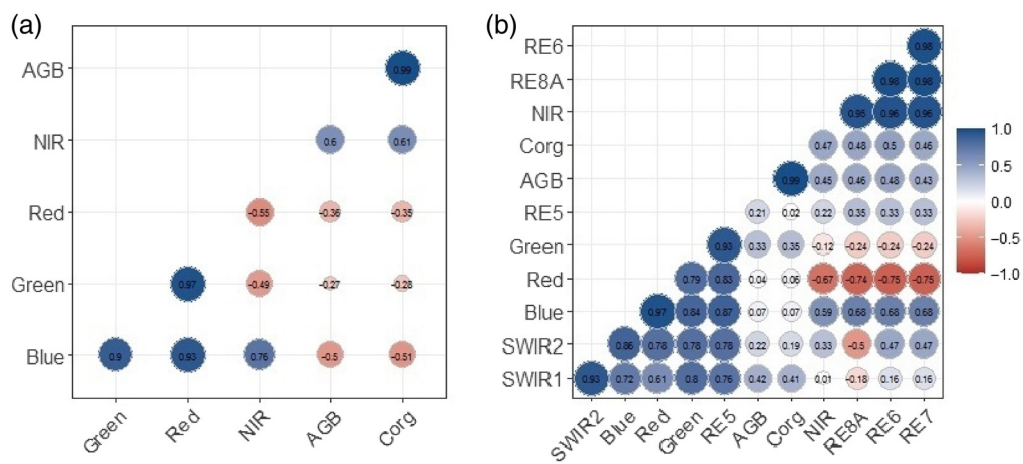


**Fig. 4** Pearson correlation coefficient matrix between the vegetation indices and biophysical variables for each sensor: (a) PlanetScope sensor and (b) Sentinel-2A sensor. AGB: aboveground biomass and Corg: organic carbon.

**Table 5** Pearson Correlation coefficient and p-values for AGB and Corg with VIs.

Index	PlanetScope sensor				Sentinel-2 sensor			
	AGB		Corg		AGB		Corg	
	<i>r</i>	<i>p</i>	<i>r</i>	<i>p</i>	<i>r</i>	<i>p</i>	<i>r</i>	<i>p</i>
NDVI	0.55	0.004	0.55	0.004	0.24	0.230	0.26	0.190
NDAVI	0.57	0.003	0.58	0.002	0.25	0.224	0.28	0.181
WAVI	0.57	0.003	0.58	0.002	0.25	0.224	0.28	0.181
sPRI	0.66	0.000	0.68	0.000	0.19	0.353	0.22	0.295
CO <sub>2</sub> Flux	0.59	0.002	0.59	0.002	0.66	0.000	0.65	0.000
CO <sub>2</sub> FluxNDAVI	0.61	0.001	0.62	0.001	0.30	0.146	0.33	0.109

Note: *p*-value < 0.05 is significant.

For the Sentinel-2A sensor, only the CO<sub>2</sub>Flux VI showed significant correlation with biophysical variables,  $r = 0.66$ ;  $0.65$ ;  $p < 0.05$ , followed by the CO<sub>2</sub>FluxNDAVI index with no significant correlation,  $r = 0.30$  and  $0.33$ . Correlations with the other indices achieved  $r$  values lower than  $0.30$ .

The VIs formed with the Sentinel-2A Red Edge bands showed no significant correlations and were therefore not entered into the correlation matrix. The highest correlation was seen with the NDRE4 index formulated with the RE5 and NIR bands,  $r = 0.30$  and  $0.32$ , for AGB and Corg. A higher correlation between the set of NDREs generated and the biophysical variables was expected since good correlations and the potential of these indices as predictive variables for wetland biomass,<sup>39,44</sup> and leaf area index are verified in different crops.<sup>71,84</sup> Changes in the position of the red edge band can occur in flood events, which could reduce the effectiveness of NDRE indices in RS applications.<sup>85</sup> However, images with the occurrence of floods or with high rainfall levels close to the date of capture of the scenes were not used.

NDAVI and WAVI showed  $r$  values greater than NDVI for both sensors. A similar result was found in Ref. 37 where the NDAVI and WAVI performed better for differentiating wetland vegetation, when compared to NDVI. This result supports the hypothesis that NDAVI can be associated with biophysical data from vegetation and used to monitor its dynamics. The substitution of NDVI by NDAVI in the VIs CO<sub>2</sub>Flux NDAVI reached a higher correlation for the PlanetScope sensor data.

The sPRI has considerable potential for mapping photosynthetic fluxes in large landscapes, in compliance with Ref. 65 The authors found a strong coefficient of determination,  $R^2 = 0.78$ , between the sPRI and carbon flux data. The CO<sub>2</sub>Flux VI was evaluated in the Ref. 86 to check the loss of carbon sequestration by vegetation before and after a fire and in regrowth. The authors verified that vegetated areas have a high CO<sub>2</sub>Flux because the plants retain more carbon dioxide, whereas the burnt areas have a low CO<sub>2</sub>Flux due to the release of carbon dioxide and because they lose part of the vegetation by burning.

The VIs CO<sub>2</sub>flux and CO<sub>2</sub>fluxNDAVI showed significant correlation in both sensors. However, the extracted values were not directly comparable between sensors, as well as for most of the VIs applied. Table 6 gives the statistics extracted in the sample site points, describing the dynamic range of the extracted values of the spectral indices common to both sensors.

The NDVI index for both sensors proved to be more sensitive to biomass variations, with a range of  $0.29$  and  $0.40$  between maximum and minimum values, respectively, followed by NDAVI for the PlanetScope sensor and WAVI for the Sentinel-2 sensor. The VIs showed similar behavior because the mean values observed were very close between sensors. However, the values of coefficient of variation (CV%), values, in majority, point to greater heterogeneity in the spectral values of Sentinel-2. The CV% measures the percentage dispersion of the data around the mean of the observed values; it is given by the percentage ratio between the standard deviation (Std) and the mean.

**Table 6** Statistics of the VIs in the sample sites on each of the sensors.

	PlanetScope				Sentinel-2A			
	Max-min	Mean	DP	CV%	Max-min	Mean	DP	CV%
NDVI	0.29	0.60	0.09	15.34	0.40	0.64	0.12	19.41
NDAVI	0.26	0.66	0.09	13.00	0.27	0.75	0.08	11.04
WAVI	0.04	0.98	0.13	13.00	0.41	1.13	0.12	11.04
sPRI	0.05	0.55	0.01	2.38	0.13	0.62	0.04	6.16
CO <sub>2</sub> Flux	0.18	0.33	0.06	17.04	0.32	0.32	0.09	26.88
CO <sub>2</sub> FluxNDAVI	0.17	0.36	0.05	14.85	0.26	0.47	0.08	16.90

It is noted that the dynamic range of the extracted PlanetScope VIs values (Max – Min) was reduced compared to the extracted Sentinel-2A VIs values, which indicates a significant positive bias in the Sentinel-2A values. This can also be verified in Fig. 5, where we use as example the VIs CO<sub>2</sub>Flux and CO<sub>2</sub>FluxNDAVI with significant correlation in both sensors. It can be seen from Fig. 5 that both sensors were sensitive to the seasonal greenness of *Scirpus giganteus* and woody and shrub species present in the study area in the summer and spring months (March and November), as well as to the lower vegetative activity in the winter months. (August).

The CO<sub>2</sub>Flux was used to test the ability of sensors to capture the *Scirpus giganteus* spectral response with a scale of 1:1300 m (Fig. 6). Compared to Sentinel, the improved spatial resolution of the PlanetScope sensor allows a more precise definition of surface details, enabling better delineation of the vegetation canopy due to higher pixel variability (see also Fig. 5), however the background effect of the soil can be more noticeable, which can lead to lower VIs values.

The Sentinel image pixel, with 10 m of spatial resolution, generalizes and tends to increase the spectral response of the vegetation in the same area, which may justify the higher values of the indices. Lower values of VIs extracted from the PlanetScope sensor were also found in Ref. 87 when comparing derived temporal NDVI profiles of PlanetScope and Sentinel-2 sensors for mapping of grassland phenology, corroborating our result.

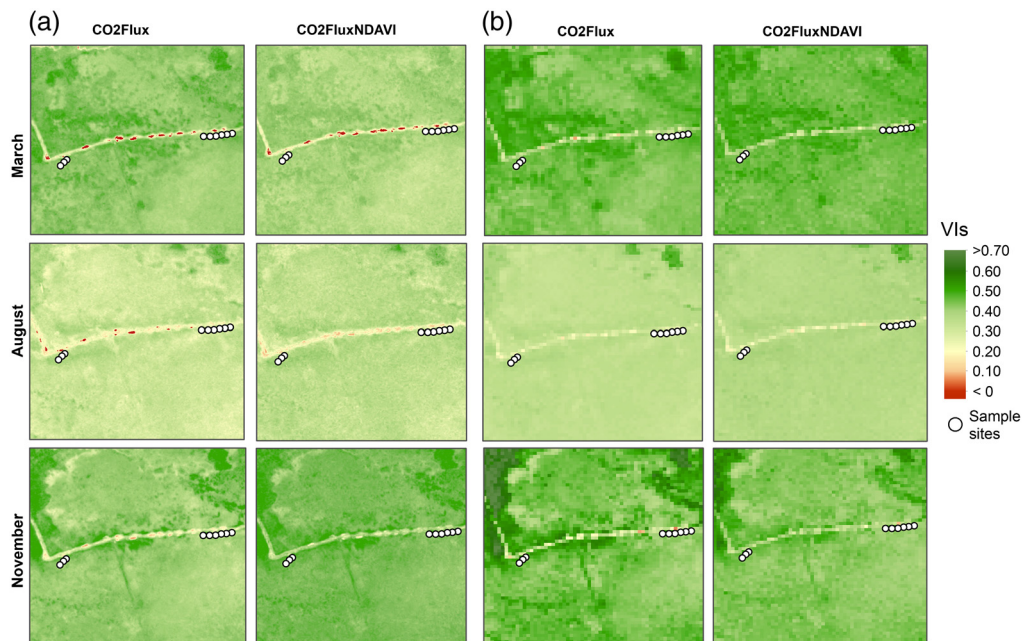


**Fig. 5** Spatialization of CO<sub>2</sub>flux and CO<sub>2</sub>fluxNDAVI VIs images on each collection date.

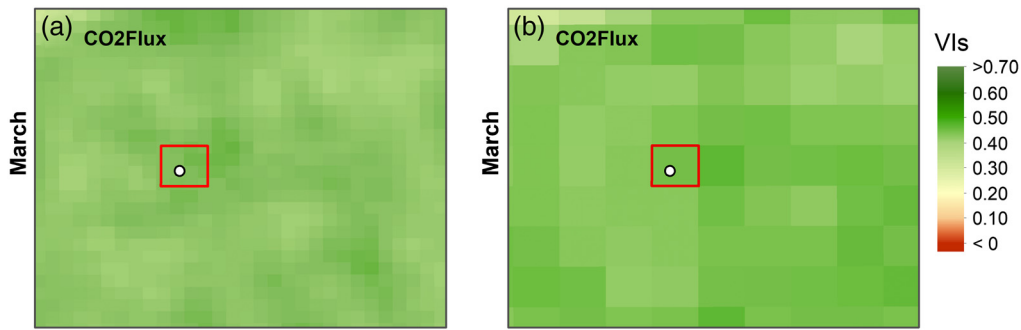


**Fig. 6** A 10-m<sup>2</sup> polygon overlaid on the sample site and CO<sub>2</sub>flux image derived from (a) PlanetScope image and (b) Sentinel image, both acquired on March 11 and 13, 2018, respectively.

### 3.2 Analysis of the Regression Models for Estimating Biophysical Variables

The best models to predict AGB and Corg from the spectral data of each sensor were selected based on the higher  $R^2$  and  $R^2_{adj}$  values, lower RMSE and ANOVA, with  $p$ -value below 0.005. Table 7 gives the equations with the best performance for estimating AGB and Corg for each sensor and their coefficients.

Simple regressions generated with PlanetScope data produced predictive RMSE = 157.10 g/m<sup>2</sup> (23.8% of mean observed AGB) and 62.77 g/m<sup>2</sup> (23% of mean observed Corg) compared to the multiple linear regression generated from Sentinel-2A data, with RMSE = 166.73 g/m<sup>2</sup> (25.3% of the mean observed AGB) and 67.47 g/m<sup>2</sup> (24.6% of the mean observed Corg).

From the values of  $R^2_{adj}$  (Table 7), it was verified that the models generated with PlanetScope data achieved greater contribution and reliability as the best predictor of AGB (42%) and Corg (44%), with higher accuracy when compared to Sentinel-2A.

Respectively, the models generated from Sentinel-2A data achieved reliability in predicting the AGB (41%) and Corg (40%) for the species *Scirpus giganteus*. The model with the best fit in the equations based on PlanetScope data occurred only with the sPRI index as the predictive variable. Models generated with a larger number of variables had lower  $R^2_{adj}$  values and higher RMSE. The opposite occurred for the equations based on Sentinel-2A data since with the inclusion of the Red Edge RE6 band in the model, in addition to the CO<sub>2</sub>Flux index, there was an increase in  $R^2_{adj}$  and lower RMSE.

A similar result was found in Ref. 72 for the AGB estimate of grassland vegetation in a marsh area. In the research mentioned, the combination of traditional bands and VIs and Red Edge and textures derived from the red edge B8, B7, B8A, and B6 bands achieved better performance in estimating AGB ( $R^2 = 0.849$ ; RMSE = 127.578 g/m<sup>2</sup>) than if those bands were used separately ( $R^2 = 0.738$ ; RMSE = 164,812). Furthermore, the four red edge bands and VIs were the most important variables for the RF and XGBoost regression prediction models.

Likewise, pursuant to Ref. 39 the best multiple regression model for estimating emergent biomass was a combined model of the red edge (band 6) and NIR1 bands from the World

**Table 7** Regression equations: (A) PlanetScope sensor and (B) Sentinel-2A sensor.

	Biop. var (g/m <sup>2</sup> )	Equation	Test $R^2$	$R^2_{adj}$	RMSE*	$p$ -value**
A	AGB	= 4896,287 + 10168,022 * sPRI	0.44	0.42	157.10	0.000
	Corg	= 2030,075+4217,391*sPRI	0.46	0.44	62.77	0.000
B	AGB	= 78,034+1409,939*CO <sub>2</sub> Flux + 1212,366*RE6	0.46	0.41	166.73	0.001
	Corg	=29,054+536,955*CO <sub>2</sub> Flux + 550,291*RE6	0.45	0.40	67.47	0.001

\*RMSE in g/m<sup>2</sup>; \*\* $p$ -value significant ( $p < 0.005$ , 95% CI).

**Table 8** Estimates of biophysical variables in g/m<sup>2</sup>, generated from models versus values observed on site.

	PlanetScope		Sentinel-2A		V. Observed	
	AGB	Corg	AGB	Corg	AGB	Corg
Min	421.81	175.71	525.43	220.10	340.24	142.9
Max.	886.39	368.41	1055.41	427.90	1289.28	502.82
Max–min	464.58	192.70	529.98	207.80	949.04	359.92
Mean	656.33	270.81	682.40	283.24	658.32	273.82
Std	136.28	56.52	145.24	57.44	201.35	81.81
CV%	20.70	20.64	21.28	20.28	30.58	29.87

View sensor. Band 6 of this sensor has a spectral range from 705 to 745 nm, the same as bands RE5 and RE6 of the Sentinel-2A sensor. The authors’ model resulted in an  $R^2 = 0.69$  and  $RMSE = 546 \text{ g/m}^2$ , 16% of the mean biomass observed.

Data from the PlanetScope sensor was used to predict AGB in a wetland with the species *Spartina alterniflora*.<sup>88</sup> In this study, the regression model that best predicted AGB used the combination of the visible difference vegetation index VIs, which includes only the visible bands, and the SAVI formulated with the NIR and red bands. This combination resulted in an  $R^2 = 0.74$  and  $RMSE = 223.38 \text{ g/m}^2$ , and was similar to the best predictive VIs seen in our study for the same sensor since sPRI and CO<sup>2</sup>fluxNDAVI are derived from combinations of visible and NIR bands.

We analyzed further the relationship between the observed and predicted AGB and Corg based on the two best models (Table 8) and are shown as scatter plots (Fig. 7). It is observed (Table 8) that the mean values estimated for the biophysical variables by the models were very close to the observed values, especially for the equations based on the spectral data of the PlanetScope sensor.

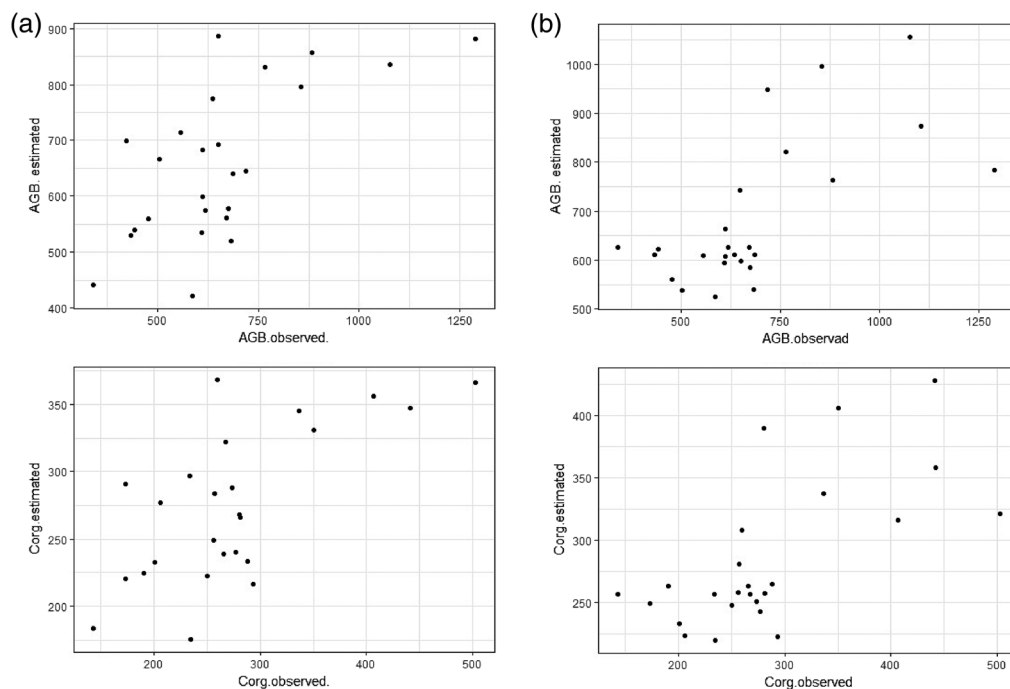


**Fig. 7** Dispersion of values estimated by the equations versus the observed values: (a) PlanetScope and (b) Sentinel-2A.

The CV% and SD values show that the variations in the estimated data were lower than the variations in observed data. These, together with the difference between the maximum and minimum values, indicate the tendency of the models to underestimate AGB and Corg. Both models had a saturation problem, which resulted in underestimation of the biophysical variables in the high biomass area, especially for the PlanetScope sensor.

Note that the Sentinel model was relatively better to estimate high AGB and Corg than the PlanetScope model (more than 169 g/m<sup>2</sup> for AGB and 59 g/m<sup>2</sup> for Corg). However, the PlanetScope model produced the lowest RMSE, and the mean estimates were closer to the actual observation. Thus, the spatially modeling of the AGB and Corg it was generated (Fig. 8) according to equation of PlanetScope from Table 7.

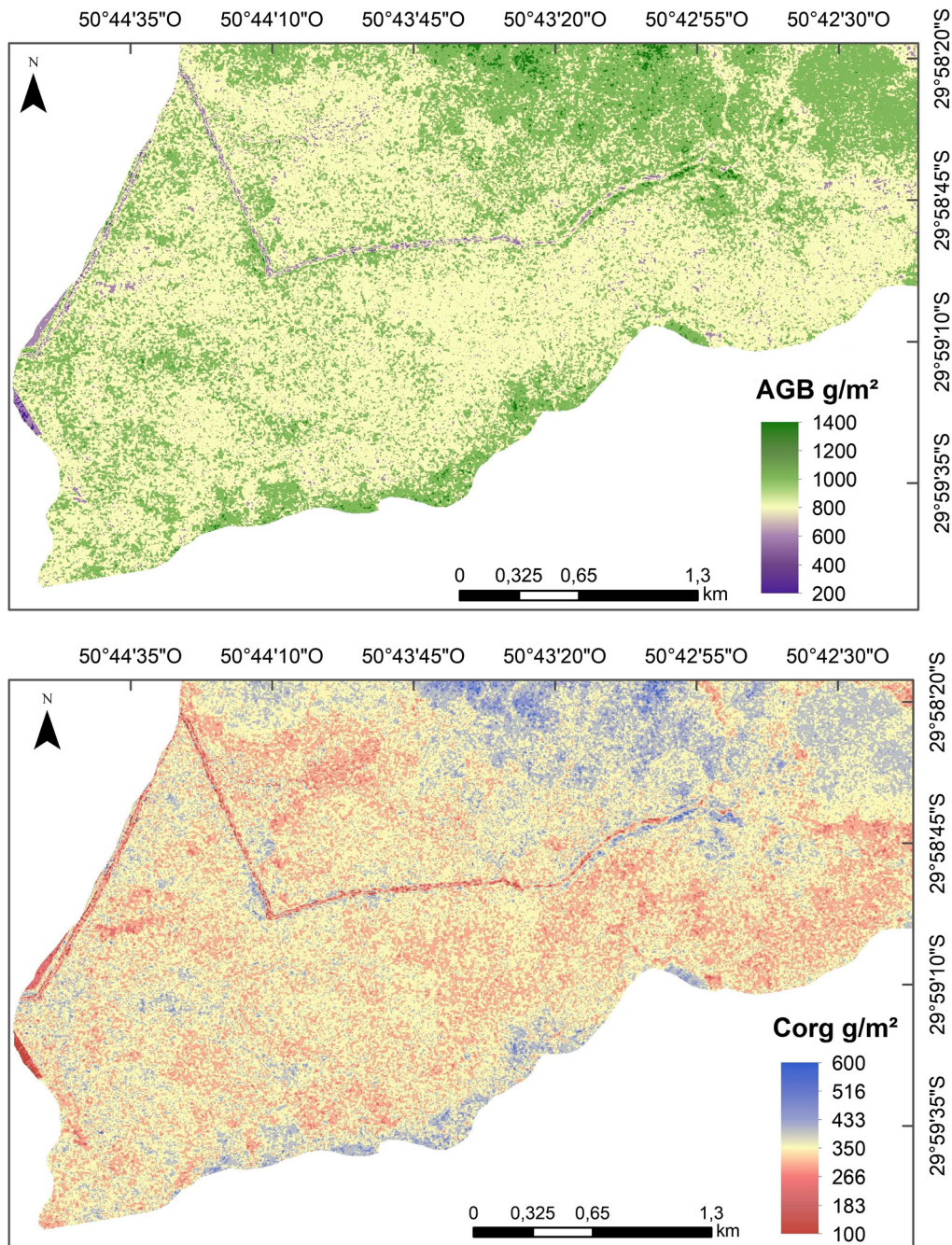


**Fig. 8** Spatial distribution of estimated AGB and Corg in the BG marsh.

The AGB and Corg maps show little spatial heterogeneity in the area covered by *Scirpus giganteus*. AGB varies between 700 and 1000 g/m<sup>2</sup> and Corg between 266 and 400 g/m<sup>2</sup>. The largest AGB and Corg are distributed in the areas with woody and shrub species. The lowest values are presented in areas with open water, flooded or more moisture.

It can be seen from the results of this study and the other studies cited that the efficiency of the PlanetScope and Sentinel-2 data as predictors of AGB and Corg is relatively higher with the use of VIs. According to Ref. 60, this is due to the potential of VIs to highlight intrinsic plant properties that are strongly related to biomass accumulation, such as greenness and leaf vigor.

Our study showed satisfactory results for estimating AGB based on Sentinel-2A. The multivariate regression model generated RMSE = 166.73 g/m<sup>2</sup>. This RMSE value is low compared to recent studies.<sup>72,83</sup> The result from PlanetScope is also satisfactory with an RMSE value = 157.10, comparable to the value obtained in Ref. 88 with RMSE = 223.38 g/m<sup>2</sup>.

In addition to providing current estimates of AGB and Corg, the use of SV has proved especially useful for monitoring and inventorying Corg stocks in marsh, which is crucial for emission offsetting and carbon credit projects, similar to the REDD programs. Furthermore, it contributes to the recognition of the environmental function of this marsh as a blue carbon ecosystem.

There are still few studies comparing the performance of the Sentinel-2 and PlanetScope sensors using AGB and Corg prediction models based on-site collected data, spectral bands, and VIs derived from these systems. As for of marsh ecosystems in southern Brazil, this is a pioneer work on the prediction of AGB and Corg from spectral data. Therefore, these findings on the relationships between biophysical variables and vegetation cover reflectance in these ecosystems are just in the beginning.

As next steps, we suggest the evaluation of other VIs and the use of time series spectral images. To improve the prediction accuracy, we suggest obtaining a larger amount of sample data and using more advanced evaluation methods, such as ensemble learning-based algorithms.

## 4 Conclusions

The relationships between the biophysical variables and the set of predictive variables were established. This study demonstrated the efficiency of spectral bands, Vis, and biophysical variables derived from Sentinel-2A and PlanetScope sensors, which are still poorly explored in this area. VIs were more correlated and preferable as predictive variables for the models. The highest and significant correlations were obtained with the sPRI VI for PlanetScope and with CO<sub>2</sub>flux for Sentinel-2A.

The NIR band presented the highest correlation with the biophysical variables for the PlanetScope Sensor, whereas for Sentinel-2A, the greatest correlation was with the red edge RE6 band. No significant correlations were observed between the NDRE indices and the biophysical variables. However, the addition of the RE6 edge band increased the  $R^2$ adj of the model for the Sentinel-2 satellite, demonstrating its capacity as a quantitative indicator of biophysical variables.

Even with a smaller number of spectral bands, the PlanetScope sensor was more efficient in predicting the variables. The model that generated the best estimate of the biophysical variables based on spectral data was the one fitted with PlanetScope data as a simple linear regression, which is unusual since in most studies multiple regression models provide the smallest errors.

Thus, the sensor with higher spatial resolution provided more contribution for the prediction of biophysical variables, generating a mean estimated AGB = 656.33 g/m<sup>2</sup> and Corg = 270.81 g/m<sup>2</sup> for the species *Scirpus giganteus* in BG, and a prediction RMSE of 157.10 and 62.77 g/m<sup>2</sup>, respectively.

Overall, the study recommends both Sentinel-2 and PlanetScope for predicting AGB and Corg in emerging marsh areas due to their low RMSE values and their contribution as predictors of biophysical variables based on  $R^2$ adj values. We conclude that Both sensors showed appreciable potential for pixel-based estimates of AGB and Corg and the VIs sPRI and CO<sub>2</sub>Flux have ability to simply and easily convey these habitat information makes it worthy of further refinement and validation as a tool for support for the management, monitoring, and conservation of marshes.

## Acknowledgments

The authors would like to thank the Gravataí Municipal Environment Foundation for Support to the field work and the aerial photos granted. This study was financed in part by the Coordenação de Aperfeiçoamento de Pessoal de Nível Superior – Brasil (CAPES) – Finance Code 001, Award no. 88887.488339/2020-00, and Research Productivity Scholarship of the National Council for Scientific and Technological Development.

## Code, Data, and Materials Availability

The datasets analyzed in this study can be found in Copernicus Open Access Hub.<sup>56,58</sup> Further inquiries about the data can be directed to the corresponding author.

## References

1. K. Ewel, R. Twilley, and J. I. N. Ong, “Different kinds of mangrove forests provide different goods and services,” *Global Ecol. Biogeogr.* **7**(1), 83–94 (1998).
2. E. L. Tabilo Valdivieso, *El beneficio de los humedales en América Central: el potencial de los humedales para el Desarrollo*, 1st ed., Vol. **58**, Turrialba, WWF-PRMS-Universidad Nacional Heredia, Costa Rica (1999).
3. E. B. Barbier et al., “The value of estuarine and coastal ecosystem services,” *Ecol. Monogr.* **81**(2), 169–193 (2011).
4. E. Mcleod et al., “A blueprint for blue carbon: toward an improved understanding of the role of vegetated coastal habitats in sequestering CO<sub>2</sub>,” *Front. Ecol. Environ.* **9**(10), 552–560 (2011).
5. C. M. Duarte et al., “The role of coastal plant communities for climate change mitigation and adaptation,” *Nat. Clim. Change* **3**(11), 961–968 (2013).
6. C. Nellemann and E. Corcoran, *Blue Carbon: The Role of Healthy Oceans in Binding Carbon: A Rapid Response Assessment*, UNEP/Earthprint, Norway (2009).
7. K. B. Byrd, “A remote sensing-based model of tidal marsh aboveground carbon stocks for the conterminous United States,” *ISPRS J. Photogramm. Remote Sens.* **139**, 255–271 (2018).
8. J. B. Kauffman et al., “Carbon stocks of mangroves and salt marshes of the Amazon region, Brazil,” *Biol. Lett.* **14**(9), 1–4 (2018).
9. D. Peteet et al., “Climate and anthropogenic controls on blue carbon sequestration in Hudson River tidal marsh, Piermont, New York,” *Environ. Res. Lett.* **15**(6), 065001 (2020).
10. S. Emmett-Mattox and S. Crooks, *Restore America’s Estuaries, Coastal Blue Carbon as an Incentive for Coastal Conservation, Restoration and Management: A Template for Understanding Options*, Bringing Wetlands to Market, Virginia (2014).
11. H. K. Gibbs et al., “Monitoring and estimating tropical forest carbon stocks: making REDD a reality,” *Environ. Res. Lett.* **2**(4), 1–13 (2007).
12. J. Chave, “Improved allometric models to estimate the aboveground biomass of tropical trees,” *Global Change Biol.* **20**(10), 3177–3190 (2014).
13. D. M. Along, “Carbon sequestration in mangrove forests,” *Carbon Manage.* **3**(3), 313–322 (2012).
14. S. Ghosh, D. R. Mishra, and A. A. Gitelson, “Long-term monitoring of biophysical characteristics of tidal wetlands in the northern Gulf of Mexico - a methodological approach using MODIS,” *Remote Sens. Environ.* **173**, 39–58 (2016).
15. IPCC (Intergovernmental Panel on Climate Change), “Supplement to the 2006 IPCC Guidelines for National Greenhouse Gas Inventories: Wetlands,” T. Hiraishi et al., 354, IPCC, Switzerland (2014).
16. Conservation International, Intergovernmental Oceanographic Commission of UNESCO, International Union for Conservation of Nature, “Coastal blue carbon: methods for assessing carbon stocks and emissions factors in mangroves, tidal salt marshes, and seagrass meadows,” J. Howard et al., 180, Virginia (2014).

17. D. A. Sani, M. Hashim, and M. S. Hossain, "Recent advancement on estimation of blue carbon biomass using satellite-based approach," *Int. J. Remote Sens.* **40**(20), 7679–7715 (2019).
18. C. Craft, et al., "Twenty five years of ecosystem development of constructed *Spartina alterniflora* (Loisel) marshes," *Ecol. Appl.* **9**(4), 1405–1419 (1999).
19. N. Saintilan, "Biogeography of Australian saltmarsh plants," *Austral Ecol.* **34**(8), 929–937 (2009).
20. L. F. C. Ruiz et al., "Object-based classification of vegetation species in a subtropical wetland using Sentinel-1 and Sentinel-2A images," *Sci. Remote Sens.* **3**, 100017 (2021).
21. J. Franklin and J. A. Miller, *Mapping Species Distributions: Spatial Inference and Prediction*, Cambridge University Press.
22. N. Zhu et al., "Mapping of biophysical and biochemical properties of coastal tidal wetland habitats with Landsat 8," *J. Appl. Remote Sens.* **15** (3), 038508 (2021)
23. W. Rongrong et al., "Modeling wetland aboveground biomass in the Poyang Lake National Nature Reserve using machine learning algorithms and Landsat-8 imagery," *J. Appl. Remote Sens.* **12**(4), 046029 (2018).
24. F. M. Rocha de Souza Pereira et al., "Reducing uncertainty in mapping of mangrove aboveground biomass using airborne discrete return LiDAR data," *Rem. Sens.* **10**(4), 637 (2018).
25. H. E. Greaves et al., "High-resolution mapping of aboveground shrub biomass in arctic tundra using airborne LiDAR and imagery," *Remote Sens. Environ.* **184**, 361–373 (2016).
26. D. A. Ventura et al., "Mapping and classification of ecologically sensitive marine habitats using unmanned aerial vehicle (UAV) imagery and object-based image analysis (OBIA)," *Remote. Sens.* **10**(1331), 1–23 (2018).
27. S. L. Powell et al., "Quantification of live aboveground forest biomass dynamics with Landsat time-series and field inventory data: a comparison of empirical modeling approaches," *Remote Sens. Environ.* **114**(5), 1053–1068 (2010).
28. M. Guo, "A review of wetland remote sensing," *Sensors*, **17**(4), 777 (2017).
29. F. J. Ponzoni, Y. E. Shimabukuro, and T. M. Kuplich, *Sensoriamento remoto da vegetação*, 2° ed., Oficina de textos, São Paulo (2015).
30. T. S. F. Silva et al., "Remote sensing of aquatic vegetation theory and applications," *Environ. Monit. Assess.* **140**, 131–145 (2008).
31. C. Guo and X. Guo, "Estimating leaf chlorophyll and nitrogen content of wetland emergent plants using hyperspectral data in the visible domain," *Spectrosc. Lett.* **49**(3), 180–187 (2016).
32. B. M. Díaz and G. A. Blackburn, "Remote sensing of mangrove biophysical properties: evidence from a laboratory simulation of the possible effects of background variation on spectral vegetation indices," *Int. J. Remote Sens.* **24**(1), 53–73 (2003).
33. K. B. Byrd, "Evaluation of sensor types and environmental controls on mapping biomass of coastal marsh emergent vegetation," *Rem. Sens. Environ.* **149**, 166–180 (2014).
34. S. Sun et al., "Modelling aboveground biomass carbon stock of the Bohai Rim coastal wetlands by integrating remote sensing, terrain, and climate data," *Remote Sens.* **13**, 4321 (2021).
35. E. Warwick-Champion et al., "Characterising the aboveground carbon content of Saltmarsh in Jervis Bay, NSW, using ArborCam and PlanetScope," *Remote Sens.* **14**, 1782 (2022).
36. T. Lillesand, R. W. Kiefer, and J. Chipman, "Digital image processing," in *Remote Sensing and Image Interpretation*, 6th ed., pp. 491–503, John Wiley & Sons, New York (2015).
37. P. Villa et al., "Comparative assessment of broadband vegetation indices over aquatic vegetation," *IEEE J. Sel. Top. Appl. Earth Obs. Remote Sens.* **7**(7), 3117–3127 (2014).
38. J. L. C. A. Davis, "Living shorelines: coastal resilience with a blue carbon benefit," *PLoS One* **10**(11), e0142595 (2015).
39. O. Mutanga, E. Adam, and M. A. Cho, "High density biomass estimation for wetland vegetation using WorldView-2 imagery and random forest regression algorithm," *Int. J. Appl. Earth Observ. Geoinf.* **18**, 399–406 (2012).
40. L. Naidoo, "Estimating above ground biomass as an indicator of carbon storage in vegetated wetlands of the grassland biome of South Africa," *Int. J. Appl. Earth Observ. Geoinf.* **78**, 118–129 (2019).

41. Y. Zhao et al., "Mapping phragmites *Australis* aboveground biomass in the momoge wetland Ramsar site based on Sentinel-1/2 images," *Remote Sens.* **14**(3), 694, (2022).
42. MultiSpectral Instrument (MSI), "Product specification," <https://sentinel.esa.int/web/sentinel/technical-guides/sentinel-2-msi/msi-instrument> (accessed 01 February 2022).
43. Planet Team Planet Imagery Product Specification, <https://assets.planet.com/docs/combinedimagery-product-spec-final-may-2019.pdf> (accessed 01 February 2022).
44. A. B. Baloloy, "Estimation of mangrove forest aboveground biomass using multispectral bands, vegetation indices and biophysical variables derived from optical satellite imageries: Rapideye, Planetscope and Sentinel-2," *ISPRS Ann. Photogramm. Remote Sens. Spatial Inf. Sci.* **4**(3) (2018).
45. J. P. D. Simioni and C. B. Etchelar, "Connectivity among wetlands of EPA of Banhado Grande, RS," *RBRH* **22**, 1–11 (2017).
46. M. G. Leite and L. A. Guasselli, "Dinâmica espaço-temporal das macrófitas aquáticas no Banhado Grande, bacia hidrográfica do rio Gravataí, RS," *Para Onde!?* **7**(1), 17–24 (2013).
47. T. F. Belloli, "Classificação baseada em objeto de tipologias de cobertura vegetal em área úmida integrando imagens ópticas e SAR," *Revista Brasileira de Cartografia.* **74**(1), 67–83 (2022).
48. D. Frantz et al., "Caracterização de ambientes paludais da planície costeira do Rio Grande do Sul em imagens orbitais TM/Landsat 5," in *VI Simpósio Brasileiro de Sensoriamento Remoto (SBSR)*, pp. 408–418, INPE, Manaus, Brasil (1990).
49. I. A. Accordis, M. Hartz, and A. Ohlweiler, "O sistema Banhado Grande como uma área úmida de importância internacional," in *Simpósio de áreas protegidas*, pp. 56–63, Universidade Católica de Pelotas, Pelotas, Brasil (2003).
50. CPRM. Companhia de Pesquisa de Recursos Minerais, "Litoestratigrafia, escala 1:1.000.000," Estado do Rio Grande do Sul. <https://geoportal.cprm.gov.br/geosgb/> (accessed December 2020).
51. M. S. Rossato, Os climas do Rio Grande do Sul: variabilidade, tendências e tipologias, 240 f. Tese. (Doutorado em Geografia). Universidade Federal do Rio Grande do Sul, Porto Alegre, Rio Grande do Sul (2011).
52. M. L. M. Pompêo and C.V. Moschini, "Biomassa das macrófitas aquáticas: o método do Quadro," in *Macrófitas aquáticas e perifíton, aspectos ecológicos e metodológicos*, M. L. M. Pompêo and C. V. Moschini, Eds., pp. 23–44, RiMa, São Carlos, SP (2003).
53. M. J. Tedesco, *Análise do solo, plantas e outros materiais*, 2nd ed., Vol. **174**, Departamento de Solos da UFRGS, Porto Alegre (1995).
54. S. Sifleet, L. Pendleton, and B. C. Murray, *State of the Science on Coastal Blue Carbon: A Summary for Policy Makers*, Vol. **11**, Nicholas Institute for Environmental Policy Solutions, Duke Univ, Durham (2011).
55. IBM Corp, IBM SPSS Statistics for Windows, Version 25.0, IBM Corp, Armonk, NY (2017).
56. The European Space Agency (ESA), "Copernicus open access hub," 2022, <https://scihub.copernicus.eu/> (accessed December 2020).
57. M. Main-Knorn, "Sen2Cor for sentinel-2," *Proc. SPIE* **10427**, 1042704 (2017).
58. Planet Labs PBC, "Planet platform," 2022, <https://www.planet.com/> (accessed December 2020).
59. J. W. Rouse et al., "Monitoring the vernal advancement and retrogradation (green wave effect) of natural vegetation," NASA/GSFC type II Report for the Period April 1973, 87, NASA, Greenbelt, Maryland (1973).
60. C. J. Tucker et al., "Red and photographic infrared linear combinations for monitoring vegetation," *Remote Sens. Environ.* **8**(2), 127–150 (1979).
61. P. Villa et al., "A remote sensing approach to monitor the conservation status of lacustrine Phragmites australis beds," *Wetlands Ecol. Manage.* **21**(6), 399–416 (2013).
62. A. Gitelson and M. N. Merzlyak, "Spectral reflectance changes associated with autumn senescence of *Aesculus hippocastanum* L. and *Acer platanoides* L. leaves. Spectral features and relation to chlorophyll estimation," *J. Plant Physiol.* **143**(3), 286–292 (1994).
63. E. M. Barnes, "Coincident detection of crop water stress, nitrogen status and canopy density using ground based multispectral data," in *Int. Conf. Precision Agric.*, Bloomington, MN, USA, Vol. 1619, p. 15 (2000).

64. J. L. Gamon, L. Serrano, and J. S. Surfus, "The photochemical reflectance index: an optical indicator of photosynthetic radiation use efficiency across species, functional types, and nutrient levels," *Oecologia* **112**(4), 492–501 (1997).
65. A. F. Rahman et al., "Modeling spatially distributed ecosystem flux of boreal forest using hyperspectral indices from AVIRIS imagery," *J. Geophys. Res. D: Atmos.* **106**(D24), 33579–33591 (2001).
66. G. M. M. Baptista, "Validação da Modelagem de sequestro de carbono para ambientes tropicais de cerrado, por meio de dados AVIRIS HYPERION," in *Simpósio Brasileiro de Sensoriamento Remoto, (SBSR)*, pp. 1037–1044, INPE, Belo Horizonte (2003).
67. X. Dai et al., "Vegetation carbon sequestration mapping in herbaceous wetlands by using a MODIS EVI time-series data set: a case in Poyang lake wetland, China," *Remote Sens.* **12**(18), 3000 (2020).
68. T. Lillesand, R. W. Kiefer, and J. Chipman, "Remote sensing and image interpretation," in *Remote Sensing and Image Interpretation*, 6th ed., pp. 491–503, John Wiley & Sons, New York (2015).
69. W. J. Frampton et al., "Evaluating the capabilities of Sentinel-2 for quantitative estimation of biophysical variables in vegetation," *ISPRS J. Photogramm. Remote Sens.* **82**, 83–92 (2013).
70. J. G. P. W. Clevers and L. Kooistra, "Retrieving canopy chlorophyll content of potato crops using Sentinel-2 bands," in *ESA Living Planet Symp.*, Edinburgh, United Kingdom, p. 8 (2013).
71. Q. Xie, "Vegetation indices combining the red and red-edge spectral information for leaf area index retrieval," *IEEE J. Sel. Top. Appl. Earth Obs. Remote Sens.* **11**(5), 1482–1493 (2018).
72. C. Li, L. Zhou, and W. Xu, "Estimating aboveground biomass using sentinel-2 MSI data and ensemble algorithms for grassland in the Shengjin lake wetland, China," *Remote Sens.* **13**(8), 1595 (2021).
73. A. Field, *Descobrimos a estatística usando o SPSS-5*, 2nd ed., Artmed, Porto Alegre (2009).
74. P. Protolongo and P. Kandus, "Dinámica de la biomasa aérea en pajonales de *Scirpus giganteus* y juncuales de *shoenoplectus californicus* em la zona frontal del bajo delta del rio Paraná (Argentina)," *Ecotropicos* **18**(1), 30–37 (2005).
75. P. Protolongo et al., "A new method for evaluating net aboveground primary production (NAPP) of *Scirpus giganteus*," *Wetlands* **25**(1), 228–232 (2005).
76. M. Hashim et al., "Above ground blue carbon sequestration capacity of Sungai Pulai estuary seagrass meadows - a satellite based method," in *Asian Conf. Remote Sens.*, ACRS, Colombo, Sri Lanka, Vol. 37, pp. 363–369 (2016).
77. M. F. Adame et al., "Carbon stocks and soil sequestration rates of tropical riverine wetlands," *Biogeosciences* **12**(12), 3805–3818 (2015).
78. T. F. Ferreira, E. H. Van Nes, and D. M. Marques, "Continuous growth of the giant grass *Zizaniopsis bonariensis* in subtropical wetlands," *Freshwater Biol.* **54**(2), 321–330 (2009).
79. M. M. Means, "Carbon storage potential by four macrophytes as affected by planting diversity in a created wetland," *J. Environ. Manage.* **165**, 133–139 (2016).
80. L. M. Sales, L. R. Mantelli, and M. D. Bitencourt, "Determinação radiométrica de biomassa macrofítica e sua correlação com valores de reflectância obtidos por sensores remotos ópticos," in *Anais XV Simpósio Brasileiro de Sensoriamento Remoto-SBSR*, p. 5860, INPE, PR, Brasil (2010).
81. J. G. Clevers and A. A. Gitelson, "Remote estimation of crop and grass chlorophyll and nitrogen content using red-edge bands on Sentinel-2 and-3," *Int. J. Appl. Earth Observ. Geoinf.* **23**, 344–351 (2013).
82. Y. Gao et al., "Estimating the biomass of unevenly distributed aquatic vegetation in a lake using the normalized water-adjusted vegetation index and scale transformation method," *Sci. Total Environ.* **601**, 998–1007 (2017).
83. S. Bhatnagar et al., "Mapping vegetation communities inside wetlands using Sentinel-2 imagery in Ireland," *Int. J. Appl. Earth Obs. Geoinf.* **88**, 102083 (2020).
84. J. Delegido et al., "Evaluation of Sentinel-2 red-edge bands for empirical estimation of green LAI and chlorophyll content," *Sensors* **11**, 7063–7081 (2011).
85. K. R. Turpie, "Explaining the spectral red-edge features of inundated marsh vegetation," *J. Coastal Res.* **29**(5), 1111–1117 (2013).

86. D. Teobaldo and G. M. Baptista, “Quantificação da severidade das queimadas e da perda de sequestro florestal de carbono em unidades de conservação do Distrito Federal,” *Revista Brasileira de Geografia Física* **9**(1), 250–264 (2016).
87. Y. Cheng et al., “Phenology of short vegetation cycles in a Kenyan rangeland from PlanetScope and Sentinel-2,” *Remote Sens. Environ.* **248**, 112004 (2020).
88. G. J. Miller, J. T. Morris, and C. Wang, “Estimating aboveground biomass and its spatial distribution in coastal wetlands utilizing planet multispectral imagery,” *Remote Sens.* **11**(17), 2020 (2020).

**Tássia Fraga Belloli** is a geographer, received her MSc degree in remote sensing (RS) and GIS from the Federal University of Rio Grande do Sul in 2019. He is currently a PhD student at the same university and course. Her research interests include the assessment and mapping of environmental functions and ecosystem services of wetlands in southern Brazil, particularly interested in RS, geoprocessing tools, and geospatial analysis platforms and their roles in supporting such efforts.

**Laurindo Antonio Guasselli** is an associate professor in Institute of Geosciences at Federal University of Rio Grande do Sul (UFRGS), and a professor of the graduate program in geography and graduate program in remote sensing at UFRGS. He is geographer, master in remote sensing, PhD in water resources and environmental sanitation from the UFRGS, respectively in 1996 and 2005. He has experience in geosciences, working with RS, geoprocessing and geoecology in the study of wetlands: marshes, lagoons, and flood areas.

**Tatiana Mora Kuplich** is a professor in the graduate program in remote sensing (RS) at Federal University of Rio Grande do Sul (UFRGS). She received her MSc degree in RS from the National Institute for Space Research (INPE) in 1994 and a PhD from the School of Geography at the University of Southampton in 2002. Post doctorate by the Laboratory of Visualization and Image Processing at the University of California in 2015. She works on the study of Brazilian biomes using RS data and techniques.

**Luis Fernando Chimelo Ruiz** received his degree in geoprocessing from the Federal University of Santa Maria in 2013, master’s and PhD degrees in remote sensing from the Federal University of Rio Grande do Sul in 2015 and 2019, respectively. He has experience in geosciences, with emphasis on geoprocessing, remote sensing, geographic information system (GIS), working mainly on the following topics, such as machine learning, pattern recognition, geographic object-based image analysis, classification, and detection of land cover and land use change.

**Diniz Carvalho de Arruda** has a degree in geoprocessing technology from the Federal University of Santa Maria (2012) and a master’s degree in remote sensing from the Federal University of Rio Grande do Sul (2016). He is currently a graduate student, PhD level, at the Federal University of Rio Grande do Sul. He has experience in geosciences, with emphasis on RS, hyperspectral RS, and geoprocessing.

**Cecilia Balsamo Etchelar** is a professor of the post-graduation course in geoprocessing at the University São Francisco de Assis in Porto Alegre, Brazil, and tutor in the Graduation in Geography course at Federal University of Rio Grande do Sul (UFRGS). She is a geographer and MSc in remote sensing from UFRGS in 2016 and 2017, respectively, and a PhD student in geography at UFRGS. Postgraduate in environmental management in industry at the State University of Rio Grande do Sul (UERGS) in 2021.

**João Delapasse Simioni** is a geographer by the Federal University of Santa Maria (2015), master in geography—environment, education and territory, by the Federal University of Rio Grande do Sul (2017). He received his PhD in remote sensing from UFRGS in 2021. He has experience in the areas of climatology, remote sensing, wetlands, flood pulse, connectivity, and environmental analysis.